Eur. Phys. J. Appl. Phys. (2013) 64: 20302
DOI: 10.1051/epjap/2013130445

THE EUROPEAN PHYSICAL JOURNAL APPLIED PHYSICS

Regular Article

AlN thin films deposited by DC reactive magnetron sputtering: effect of oxygen on film growth

Javier García Molleja[1,2,a], Bernardo José Gómez[2], Julio Ferrón[3], Eric Gautron[1], Juan Bürgi[2], Bassam Abdallah[1,4], Mohamed Abdou Djouadi[1], Jorge Feugeas[2], and Pierre-Yves Jouan[1]

[1] Institut des Matériaux Jean Rouxel (IMN – Université de Nantes, UMR CNRS 6502), 2 rue de la Houssinière, BP 322298, 44322 Nantes Cedex 3, France
[2] Instituto de Física Rosario (CONICET-UNR), 27 de Febrero 210 bis, S2000EZP, Rosario, Argentina
[3] Instituto de Desarrollo Tecnológico para la Industria Química (INTEC-UNL), Güemes 3450, S3000GLN, Santa Fe, Argentina
[4] Physics Department, Atomic Energy Commission of Syria (AECS), 17th Nissan street, Kafar Soh, BP 6091, Damascus, Syria

Received: 26 September 2013 / Accepted: 3 October 2013
Published online: 15 November 2013 –

Abstract. Aluminum nitride is a ceramic compound with many technological applications in many fields, for example optics, electronics and resonators. Contaminants play a crucial role in the AlN performance. This paper focuses mainly in the effect of oxygen when AlN, with O impurities in its structure, is grown on oxidized layers. In this study, AlN thin films have been deposited at room temperature and low residual vacuum on SiO_2/Si (1 0 0) substrates. AlN films were grown by DC reactive magnetron sputtering (aluminum target) and atmosphere composed by an argon/nitrogen mixture. Working pressure was 3 mTorr. Film characterization was performed by AES, XRD, SEM, EDS, FTIR, HRTEM, SAED and band-bending method. Our results show that oxidized interlayer imposes compressive stresses to AlN layer, developing a polycrystalline deposition. Indeed, when film thickness is over 900 nm, influence of oxidized interlayer diminishes and crystallographic orientation changes to the (0 0 0 2) one, i.e., columnar structure, and stress relief is induced (there is a transition from compressive to tensile stress). Also, we propose a growth scenario to explain this behaviour.

1 Introduction

Aluminum nitride (AlN) is a material particularly interesting when it is used as thin film coating. This III-V compound has various technological and industrial applications such as: optics [1], mechanics [2] or electronics [3,4]. In the field of electronics there is a particular interest because of AlN has a semiconductor behaviour when is doped, but it has excellent dielectric properties when doping is avoided [5]. Moreover, AlN is a piezoelectric material with a high sound speed [6]. Aluminum nitride, with a density of 3.3 g/cm^3, is one of the best materials generating vibrations at very high frequencies. This is the reason for the good surface acoustic waves (SAW) propagation in AlN thin films, and their adaptation for the construction of bulk acoustic wave resonator (FBAR) devices, high-pass filters and pressure gauges [7–9] with them.

Among published works dedicated to synthesis of AlN thin films, several physical methods such as pulse laser deposition (PLD) [10] and more recently high-power impulse magnetron sputtering (HiPIMS) [11,12] have been used. In this study, the "classical" PVD (plasma vapour deposition) technique, based on the use of a magnetron device [13–15], was selected since well-crystallised films can be synthesized with this technique at low temperatures with high deposition rates. Indeed, PVD is also compatible with typical industrial processes used to the date.

However, the problem of oxygen addition in the structure, is still a matter of interest. For example, oxygen plays a crucial role concerning to the electrical and optical properties [16]. Moreover, interface oxides induce residual stresses to the film deposited over them. Thus, it could be interesting to know how O affects the columnar development in AlN films and the evolution of the related residual stresses. These questions are important in the industrial community, due to the poor vacuum control in the huge coating reactors employed and the cost to obtain ultra-clean substrates.

In this paper, we have studied how residual oxygen has an effect to growth process in AlN films deposited over oxidized substrates. Besides, we have analysed the relationship between residual stress development and crystallographic orientation [17]. Finally, a growth scenario which attempts to describe the growing process under this conditions is proposed.

[a] e-mail: javier.garcia-molleja@cnrs-imn.fr

2 Experimental part

2.1 Deposition process

AlN films were deposited by DC reactive magnetron sputtering at room temperature. Reactor was made of stainless steel and it has a volume of 9.4 L. The unbalanced magnetron (Minimak) was used with an Al (99.9% of purity, 1.3 inches of diameter) cathode energized by a variable power supply (FUG MCN 700-1250).

Target-substrate distance was 3 cm. In order to obtain AlN films with O contamination, base pressure was fixed to 2×10^{-5} Torr. Before each deposition, Al target was cleaned in a pure argon discharge during 10 min and then pre-sputtered in argon/nitrogen discharge for another 10 min. A shutter was used to avoid substrate contamination.

Si (1 0 0) samples, cleaned by ethanol and acetone and dried with nitrogen, were employed as substrates without biasing. This cleaning process does not suffice to erode the upper layer of SiO_2. We intentionally conserve this oxide film to study residual stress development in AlN films deposited on this Si/SiO_2 substrate. This AlN film will be affected by this amorphous layer and authors believe that this is a good point to give some insight into this field.

AlN films were deposited at 3 mTorr of working pressure. The reactive atmosphere was composed by 30% of molecular nitrogen and 70% of argon, i.e., $p_{N_2}/(p_{Ar}+p_{N_2}) = 0.30$. Voltage and current were adjusted to deposit films with a constant power of 100 W. Under these conditions, deposition rate is ≈40 nm/min.

2.2 Characterization techniques

Element concentration profiles with depth were determined using Auger electron spectroscopy (AES), with a Perkin Elmer (PHI) scanning Auger microscope mod. 590A apparatus.

Films were characterized by X-ray diffraction (XRD) analyses in the $\theta/2\theta$ scanning mode, using a CuKα source (Siemens D5000).

Surface morphology and film thickness were characterized by scanning electron microscopy (SEM) using a JEOL-type JSM6400F equipment.

Chemical composition of thin films was determined by energy dispersive spectroscopy (EDS) with a PGT IMIX-PTS probe operating at 10 kV and transmission Fourier transform infra-red (FTIR) analyses were performed with a Bruker Vertex 70 equipment with a resolution of 4 cm^{-1}.

Fine structural study of AlN films was carried out by high resolution transmission electron microscopy (HRTEM) with a Hitachi HF 2000 device. Acceleration voltage was 200 kV with a resolution of 0.23 nm. In order to do this detailed characterization, samples were thinned using a tripod polisher with diamond paper followed by ion beam milling. Additionally, electron diffraction and dark field imaging were used to analyse the microstructure and to provide information concerning the preferred orientation in the film.

Selected area electron diffraction (SAED) patterns were taken using a circular aperture with a diameter of approximately 400 nm.

Residual stresses in our AlN films were calculated by the band-bending method [18,19], where the radius of the bent, coated substrate was measured before and after deposition using a Veeco Dektak 8 profilometer. The stress was calculated by using the simplified form of Stoney's formula [20]:

$$\sigma = \frac{E_s e_s^2}{6(1-\nu_s)e_f}\left(\frac{1}{R}-\frac{1}{R_0}\right), \quad (1)$$

where R_0 and R are the radii of curvature before and after deposition, respectively; e_s and e_f are the thicknesses of the silicon substrate (= 250 μm) and the AlN film, respectively, and E_s (= 131 GPa) and ν_s (= 0.27) are, respectively, the Young modulus and the Poisson's ratio of the silicon substrate.

3 Results and discussion

3.1 Experimental characterization of AlN films

3.1.1 AES and EDS characterization

AlN-film element concentration profiles were studied using AES and EDS. First of all, an Auger spectrum was taken on the surface, and then at different depths of the film, sequentially removing layers of material by sputter of Ar^+ ions. This procedure has allowed obtain the concentration of each element at different depths down to the maximum explored depth, i.e., ∼1100 nm (corresponding to 450 min of sputtering). On Figure 1 we can see concentration profiles of each element with depth, from surface to substrate going through the interface. In zone 1

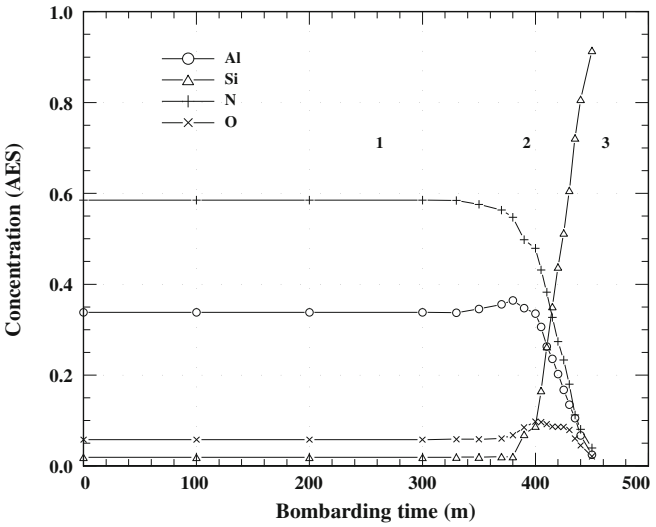

Fig. 1. AES profile with depth (i.e., sputtering time with Ar ions). Al, N, Si and O elemental concentrations are plotted. Zone 1: film, zone 2: interface, zone 3: substrate.

Table 1. Oxygen contamination, as determined by EDS, versus thickness for AlN films deposited at 3 mTorr of working pressure.

Film thickness (nm)	250	335	600	800
Oxygen atomic content (%)	5.0–6.2	4.9	2.6	2.0

(AlN thin film) we can detect an aluminum concentration of ≈34 at.% and almost 58 at.% of nitrogen, so the composition of the film is overstoichiometric. Oxygen concentration of ≈6 at.% can be seen in the whole thickness (approximately 1000 nm) [21] and this is caused by the selected residual vacuum. At the interface (zone 2), while Al concentration grows up to ≈36 at.%, O concentration grows up to ≈10 at.%, due to the presence of surface oxides. At his stage, formation of Al-O compounds is more probable than Al-N compounds because of the different values of enthalpy of formation. After that zone, oxygen (and the other elements, too) goes down to zero concentration at the substrate (zone 3). In this paper, it is not intended to develop piezoelectric devices. The purpose was to know how is the stress development in AlN films deposited at this very condition and their behaviour under this oxygen concentration.

Also, from EDS results in other AlN films (see Tab. 1) interesting data can be observed. There was an increase of the film thickness that leads to a decrease of the oxygen percentage. O contamination was about 6.2% for a film of 250 nm thick, but when film thickness was 800 nm oxygen concentration was only 2%. Thickness of the oxidized amorphous layer located at the interface is estimated in 5 nm. So, when AlN coating is very thin EDS detects this interfacial layer and leads therefore to such a high value of the oxygen content. Then, as the thickness increases, the detection of this interfacial layer becomes weaker and a decrease in the oxygen atomic percentage can be observed. This fact is qualitatively consistent with AES results.

3.1.2 Film stress

Residual stress evolution as a function of AlN-film thickness is presented on Figure 2. Residual stress is compressive in films with thicknesses ranging between 0 and 0.9 μm. In the region between 0 nm and 150 nm growing compressive stress values are measured, and for the AlN film of 150 nm thick maximum compressive stress (= 2.2 GPa) is reached. After this point, AlN films with thickness between 150 nm and 900 nm has compressive stresses, but stress values have a descending trend. For films thicker than 0.9 μm, residual stress becomes tensile. It is worth noting that the presence of a maximum of stress for sputtered films has already been reported in other papers. Indeed, similar results were observed by Nouveau et al. [22] for CrN films and by Zeitler et al. [23] for BN films. Nouveau et al. found that compressive stress is always present in their CrN films. There is a stress maximum value (6.3 GPa) in films of 170 nm thick, and an important decrease is present in thicker films, i.e., there

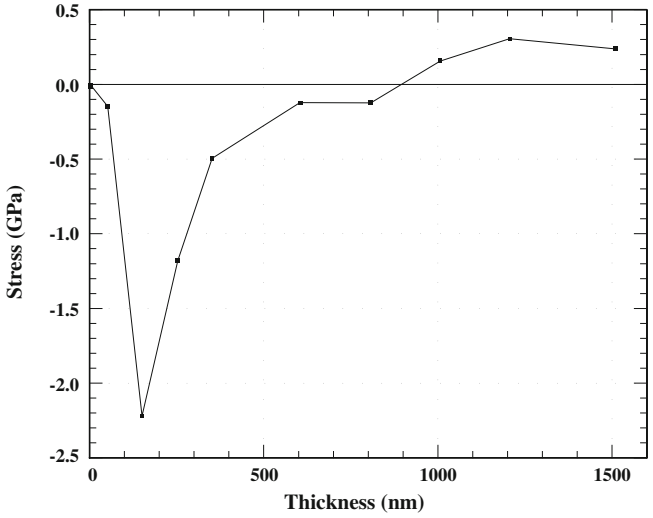

Fig. 2. Residual stress as a function of AlN film thickness. Discharge pressure of 3 mTorr.

is a development of transition from a dense structure to a less compact one. Zeitler et al. have deposited BN films at 350 °C and tensile stresses at thicknesses between 0 and 15 nm have been confirmed. Thicker films only have compressive stress. BN film of 100 nm thick has a maximum peak of stress (4.5 GPa) and after this point it is observed little stress decrease. Although, in AlN films, there is a relationship between the maximum of residual stress and film densification [19,24–27], the existence of the former is not still well understood yet.

The stress evolution previously described, i.e., from compressive stress towards tensile one, was also observed by Martin et al. [28] for AlN thin films. Martin et al. stated that AlN films with thickness between 35 nm and 1 μm had compressive stresses while thicker films had tensile stresses. Other interesting conclusion was that compressive stress decreases with thickness; results in the present paper show that there is a compressive stress increasement, reaching a maximum value at 150 nm thick and for higher thicknesses compressive stress decrease is observed. When the AlN-film thickness increases appearance of a columnar structure can be observed. It is worth to notice that the presence of O at the interface can affect significantly the grain size [29] and may explain the compressive stress development measured in the beginning of AlN film growth. When the influence of the amorphous layer is lowered, columnar structure can be developed and this structure is responsible of stress relief [19].

3.1.3 XRD characterization

It is interesting to see if the changes of residual stresses with thickness have some correlation with the crystalline structure developed. Figure 3i presents the XRD diffractograms for three thicknesses: 80 nm, 150 nm and 250 nm. For such thicknesses, we can observe that AlN films are not well crystallised due to the influence of interfacial oxygen [29]. Thus, XRD patterns exhibit two diffraction

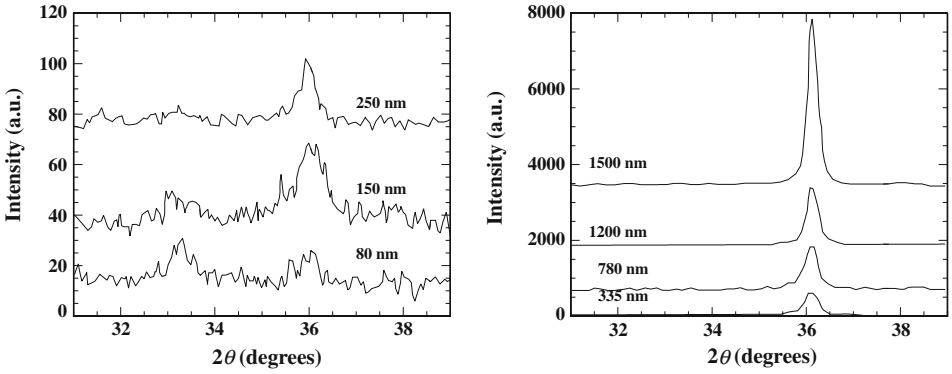

Fig. 3. XRD patterns of AlN films for different thicknesses: (i) 80 nm, 150 nm and 250 nm; (ii) 335 nm, 780 nm, 1200 nm and 1500 nm.

peaks, located at 2θ values of 33.2° and 36.1°. These positions are associated to $(1\,0\,\bar{1}\,0)$ and $(0\,0\,0\,2)$ AlN planes, respectively.

For thicknesses higher than 335 nm, $(0\,0\,0\,2)$ peak becomes more intense (Fig. 3ii) revealing a preferential orientation in the growing process. For film thicknesses higher than 780 nm, only the peak associated to the $(0\,0\,0\,2)$ plane remains, thus a definite texture in the film is achieved. This process can be explained as the competition between different preferential orientations when the influence of interface oxygen is diminished during growth: in the early stages of the film growth, AlN is polycrystalline because of it is formed by crystallites with different orientations; some growth planes can be extinguished or hampered by other planes with higher growth rate [30]. This is the reason why under our experimental conditions $(0\,0\,0\,2)$ texture is developed when film is grown. The influence of O located in the film might be lowered by the high quantity of nitrogen in the film [17]. Indeed, this texture develops a columnar structure and this fact produces stress relief. This statement can be compared with experimental results of Figure 2: films with little thickness have compressive stresses and these stresses are relieved when films have a higher thickness.

Moreover, there is a change in the FWHM of the $(0\,0\,0\,2)$ diffraction peak. For AlN film with 80 nm thick, FWHM (full width at half maximum) has a value of 0.8°, meanwhile for AlN film with 1.5 μm thick, this value decreases to 0.19°. This evolution means a better crystalline quality of the films.

3.1.4 SEM analysis

In order to have some insight in such variation of orientation, the film morphology was characterized by SEM. Figure 4i shows the cross-section of a 150-nm AlN film. This sample exhibits a dense structure, in coherence with the presence of polycrystalline structure provoked by the high O concentration at the interface.

Figure 4ii shows the cross-section of AlN 1.5-μm-thick film. The typical $(0\,0\,0\,2)$ columnar structure of sputtered films is observed. The residual stress measured for that film is very low, in the range of 200 MPa. While the

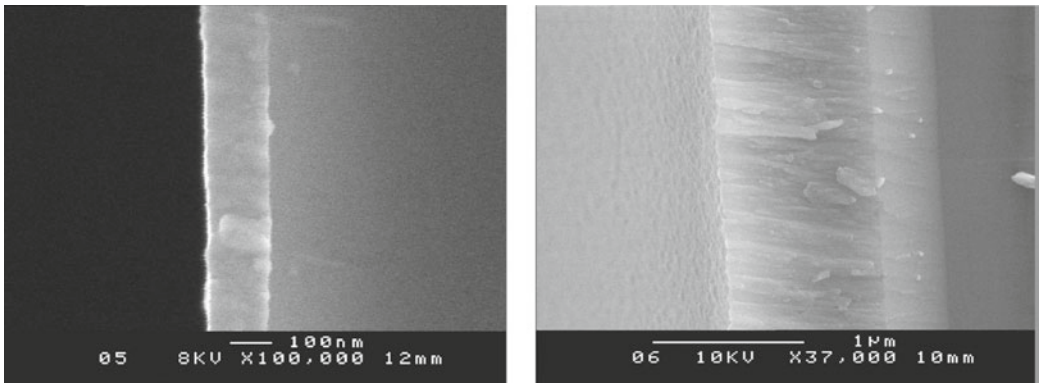

Fig. 4. Cross-sectional SEM image: (i) dense AlN films with 150 nm thick, (ii) well crystallised AlN films with columnar structure. Thickness equal to 1500 nm.

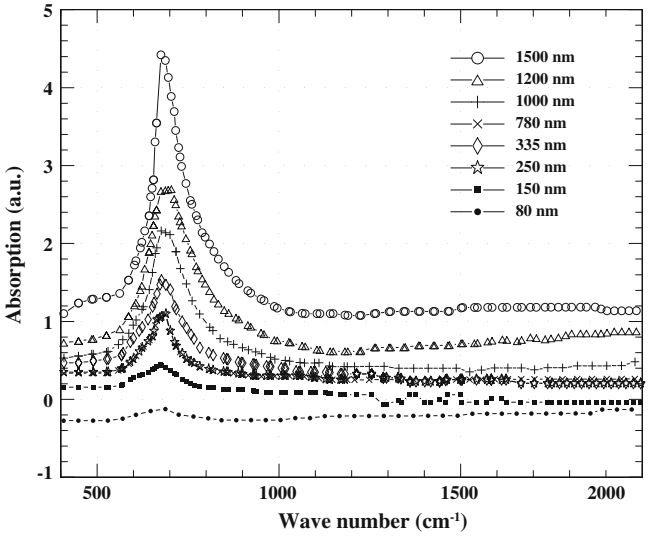

Fig. 5. FTIR transmittance spectra of AlN thin films with thickness ranging from 80 nm to 1500 nm.

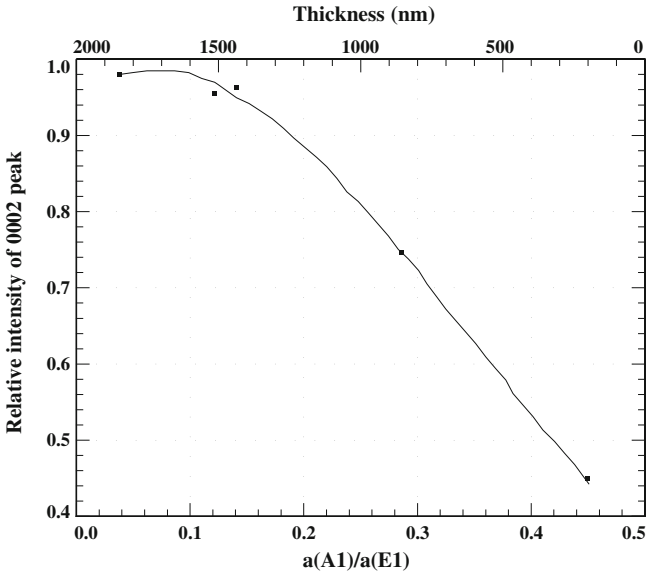

Fig. 6. Relation between IR vibrational properties and preferential orientation for polycrystalline AlN thin films. $a(\mathrm{A1})/a(\mathrm{E1})$ represents the ratio of integrated areas of the A1(TO) vibrational mode over the E1(TO) mode; the (0 0 0 2) orientation degree was obtained for each XRD pattern as the ratio of the integrated area of the (0 0 0 2) peak over the summation of the integrated areas of all the peaks present in the pattern. Line is only a guide for the eye.

first film (Fig. 4i) has a maximum (2.2 GPa) compressive stress, the second one (Fig. 4ii) has a tensile stress.

3.1.5 FTIR analysis

FTIR is an effective technique to investigate characteristic vibrational modes of the lattice. Figure 5 shows FTIR transmittance spectra of AlN thin films with thicknesses ranging from 80 nm to 1500 nm. Silicon signal has been considered as background and thus substracted from the spectra. Two characteristic modes located at 620 cm^{-1} and 670 cm^{-1} are clearly recorded. These peaks can be respectively associated to A1(TO) and E1(TO) modes, according to the literature [31]. The two vibrational modes E1(TO) and A1(TO) correspond, respectively, to the modes excited by both, electric fields perpendicular and parallel to the c-axis of the crystallite. We notice that an increase of the film thickness implies an increase in the intensity of the peak associated to the E1(TO) mode. Comparing with previous results, an increasement of E1(TO) mode with thickness is related to the development of columnar structure with a (0 0 0 2) preferential orientation and the presence of tensile stresses.

On the other hand, there is a decrease in the FWHM of the peak associated to the E1(TO) mode: when the AlN film is 80 nm thick its FWHM is 90 cm^{-1}, and when the AlN has a thickness of 1.5 μm its FWHM is 60 cm^{-1}, revealing a well crystallised structure. That is, FWHM reduction is a clue to confirm an improvement of the crystalline quality of the deposited film.

Correlation between the XRD and FTIR analyses is presented on Figure 6. This figure shows the relative intensity of the (0 0 0 2) peak (intensity of this peak over the summation of the intensities of all peaks appearing in the spectra) as a function of the ratio $a(\mathrm{A1})/a(\mathrm{E1})$, where $a(\mathrm{A1})$ and $a(\mathrm{E1})$ are the integrated area of the A1(TO) and E1(TO) vibrational modes, respectively. They are obtained from the deconvolution of each Lorentzian peak. In this figure, the highest (0 0 0 2) relative intensity with a low $a(\mathrm{A1})/a(\mathrm{E1})$ ratio can be seen, that is, the (0 0 0 2) peak prevails when thickness is over 1 μm.

According the figure, this ratio is very small (< 0.2) for films exhibiting only the (0 0 0 2) orientation in their XRD pattern. That result means that E1(TO) mode is very strong and this indicates that (0 0 0 2) texture is favoured during growth, in accordance with the loss of influence from the interface. Our results are in good agreement with previous works [31]: Sanz-Hervás et al. showed a (0 0 0 2) relative intensity of ≈ 1 when $a(\mathrm{A1})/a(\mathrm{E1})$ ratio was < 0.18 and there was a fast (0 0 0 2)-relative-intensity decrease when that ratio had higher values. However, orientations found in that paper are (0 0 0 2) and (1 0 $\bar{1}$ 2). Instead, in the present case (0 0 0 2) and (1 0 $\bar{1}$ 0) orientations are measured.

3.1.6 Analysis by HRTEM

HRTEM technique is used to explain the structural variation at different thicknesses in the same film. This HRTEM characterization has been done in the thickest AlN sample (1.5 μm). Such a film is representative for all thicknesses that we have been studied, i.e., each thickness analysed in this film is like analyse AlN films with this same thickness. Figure 7i shows the sample's cross-sectional TEM image. HRTEM images show first an amorphous Si-AlN interface (Fig. 7ii) of about 5 nm with high amount of O. This layer is due to the reaction of Al with the surface native oxide

at the beginning of the deposition. Then, this amorphous layer is followed by a polycrystalline AlN layer where crystallites are mostly $(1\,0\,\bar{1}\,0)$-oriented (see Fig. 7iii) due to the influence of the subjacent Al-O interlayer. Moreover, a few of these crystallites are $(0\,0\,0\,2)$-oriented. Grain size in this zone is of about 8 nm.

At higher thicknesses film presents a columnar structure. The so-called base of the column (Fig. 7iv) shows high quantity of $(0\,0\,0\,2)$-oriented crystallites with a grain size bigger (about 40 nm) than the ones of Figure 7iii. Perhaps, the nitrogen overstoichiometry plays some role in this grain coarsening. The remaining crystallites are $(1\,0\,\bar{1}\,0)$-oriented. The central zone of the columnar structure contains only columnar grains with $(0\,0\,0\,2)$ orientation (Fig. 7v). A tilt between the c-axis and the normal of $\sim 6°$ can be measured. In the topmost region of the columns $(0\,0\,0\,2)$ orientation is also exhibited and tilting tends to be zero (Fig. 7vi).

Interplanar spacing, corresponding to the $(0\,0\,0\,2)$ family planes and the $(1\,0\,\bar{1}\,0)$ ones, were measured. In the first case d-spacing is 0.251–0.254 nm and for the latter case is 0.2697 nm. These values are very close to their standard JCPDS ones (25-1133): $a = 3.1114$ Å, $c = 4.9792$ Å, $d_{10\cdot0} = 0.2695$ nm, $d_{00\cdot2} = 0.2490$ nm and $d_{10\cdot1} = 0.2371$ nm. These observations show that there is an enhancement of the crystalline quality as the film thickness is increased: in the beginning, over the amorphous interlayer an AlN film is grown, composed by crystallites with different orientations and their compressive stress is high because of interfacial oxygen; when film thickness is bigger there is a loss of oxygen influence and nitrogen and aluminum can combine together without imposition of the interface and thus, a columnar structure is developed. Finally, when $(0\,0\,0\,2)$ orientation prevails, stress relief is developed and interplanar spacings are similar to the tabulated ones. This description is coherent with previous characterizations.

3.1.7 SAED characterization

Selected area electron diffraction (SAED) technique was performed on the samples in order to show their crystalline features. This characterization was conducted with a circular diffracting area of 400 nm in diameter. Figure 8 shows SAED analyses of four different zones in an AlN film of 1.5 μm thick. These zones are highlighted in the TEM image of Figure 8i.

The first SAED pattern (Fig. 8ii, zone identified as point b in Fig. 8i) shows two intense rings, corresponding to the $(0\,0\,0\,2)$ and $(1\,0\,\bar{1}\,0)$ planes. Moreover, there is a misaligned angle of 35° for the $(0\,0\,0\,2)$ orientation confirming the polycrystalline nature of this zone. The second SAED pattern (Fig. 8iii, located at point c in Fig. 8i) shows a columnar high texture in the $(0\,0\,0\,2)$ plane with a misoriented angle of 25°. The following region, labeled as d in Figure 8i, has a SAED pattern represented in Figure 8iv. Columnar grains with a misaligned angle of 21° can be seen. The last SAED pattern (Fig. 8v) shows the top of the column (region e in Fig. 8i). This pattern only presents two intense spots separated by an angle of 6°, which gives to us an insight of the crystalline quality improvement.

Finally, a good agreement between the XRD, FTIR and HRTEM analyses can be observed. These characterization methods confirm the orientation of the film along the $(0\,0\,0\,2)$ c-axis as the thickness increases.

3.2 Growth scenario proposal

On the basis of these results, the following growth scenario can be proposed. At the very beginning of the growth, the AlN film deposited by PVD at room temperature consists of an amorphous interfacial layer. This oxidized layer, as confirmed by HRTEM analysis (Fig. 7ii), is followed by another layer with isotropic growth of small islands, which are affected by the compressive stresses of the subjacent layer. Each of these islands exhibit different crystal orientations and this behaviour is revealed with a high degree of confidence by HRTEM (Fig. 7iii) and XRD (Fig. 3i) techniques. When the film thickness is higher than a few hundreds of nanometers there is a loss of influence from the interface layer, therefore AlN growth becomes anisotropic and perpendicular to the substrate, showing preferential orientation along the c-axis one. This trend leads to a texturation of the layer, as confirmed by HRTEM (Fig. 7v), XRD (Fig. 3ii) and FTIR (Fig. 5) measurements.

On these bases, we can postulate that at the very beginning of the growth, all the crystalline orientations coexist over the oxidized layer. This amount of O induces compressive stress on these crystallites which is the reason to the multiple orientations obtained at this point. When the thickness is located between 250 nm and 780 nm, some orientations begin to disappear and only one orientation remains, leading to a textured film. This behaviour is triggered by the loss of influence from the oxidized interlayer. Dynamic stress profile shows that residual stress is very high at the beginning of growth, when all orientations coexist. Then, when the film crystallinity and texture are improved, residual stress strongly decreases. Our results prove that oxygen contained in the AlN film is high ($\approx$6 at.%), but it cannot affect the different stages of columnar growth; beyond the region of interface influence, the transition from compressive stress to tensile stress is similar to AlN films without O contaminant in their structure [28]. Thus, only substrate can affect on this behaviour.

When AlN film thickness is over 600 nm, the texture develops a columnar structure and compressive stress is inhibited. At the end of the process, only tensile stresses are present. This assumption of a relationship between structure and stress has been already validated for BN and CrN films but it remains to be confirmed in the case of the AlN films. Reference [28] reports relationships between FWHM, reticular distance $d_{00\cdot2}$ and thickness. Indeed, Martin et al. have shown a relationship between thickness and residual stresses. Therefore, HRTEM and SAED analyses from the present paper are good complements of these results.

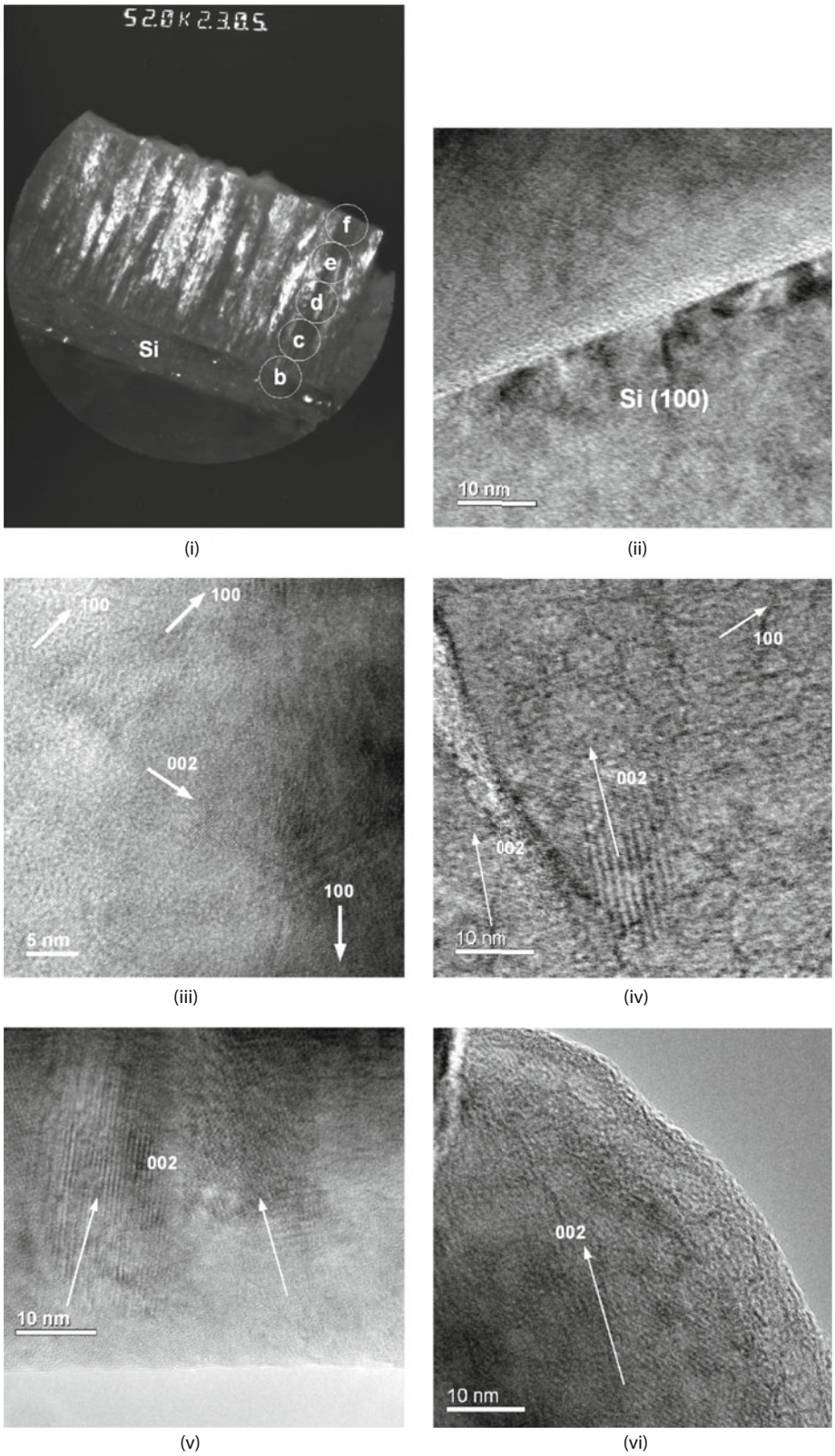

Fig. 7. (i) Cross-sectional dark field TEM image of an AlN film of 1500 nm thick deposited on Si substrate. Localized HRTEM analysis corresponds to different points of Figure 7i, (ii) point b of the figure located at the interface, (iii) point c located at 60 nm over the interface, (iv) point d, that identifies the base of the column, (v) point e represents the middle of the column and (vi) is the top of the column, identified by the point f. Arrows are normal to the indicated planes.

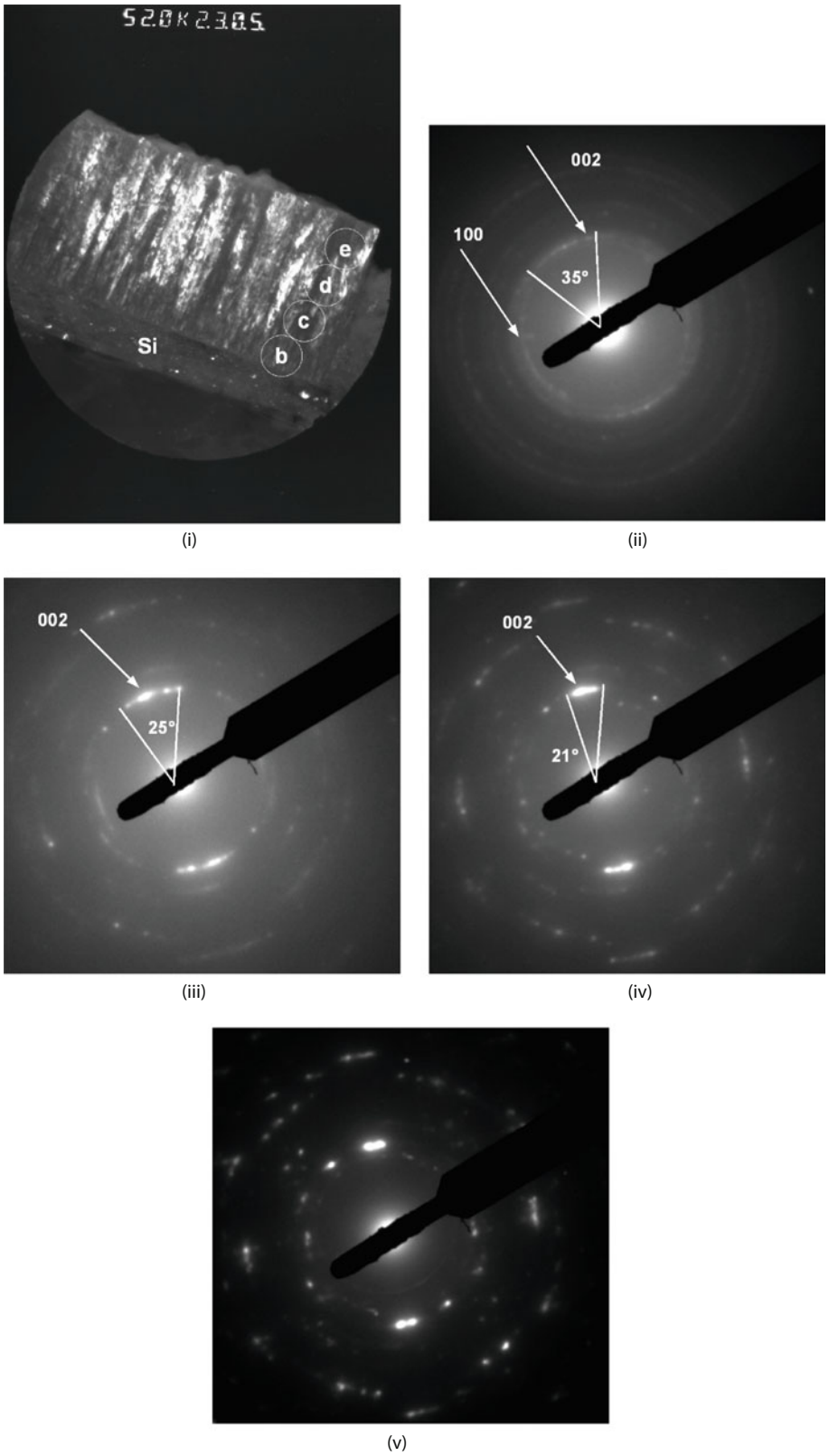

Fig. 8. (i) AlN-film cross-sectional TEM analysis. Localized SAED patterns corresponding to different points of Figure 8i, (ii) point b: interface (0–400 nm), (iii) point c: polycrystalline zone (400–800 nm), (iv) point d: base of the structure column (800–1200 nm) and (v) point e: top of the column (1200–1500 nm).

4 Conclusion

AlN thin film deposition on SiO_2/Si (1 0 0) has been done at room temperature and low pressure with DC reactive magnetron sputtering. A dynamic stress profile highlighted the existence of a peak of compressive stress for films with 150 nm thick induced by the oxidized interlayer. This amorphous film with an oxygen content of 10 at.% was shown by HRTEM analysis. Following this amorphous layer there was another one where three crystallographic orientations coexist: $(1\,0\,\bar{1}\,0)$, (0 0 0 2) and $(1\,0\,\bar{1}\,1)$. This polycrystalline region is caused by the influence of the oxidized interlayer. Consequently, the isotropic structure is related with high compressive stresses.

AES has shown that O concentration in the film was 6 at.% and AlN films were overstoichiometric (58 at.% of nitrogen), but these concentrations have not had influence in the growth process. When AlN film had a thickness of $\geq$0.9 μm, influence from the O interlayer is loss and growth became anisotropic along the *c*-axis direction. The columnar structure tended to aling along the (0 0 0 2) direction, i.e., columns perpendicular to the substrate. FTIR and XRD analyses confirmed this growth behaviour.

Finally, a growth scenario was proposed based on these experimental evidences. The oxidized interlayer determined the residual stress evolution. Transition from compressive stress to tensile stress changed the film texture. Besides, the presence of a maximum of compressive stress could be related to this O interlayer.

The combination of specific literature and this paper could give an insight about the relationship between structure and stress.

This work was subsidized by Centre National de la Recherche Scientifique (France) and Consejo Nacional de Investigaciones Científicas y Técnicas (Argentina) under Resolution number 962/07-05-2009. Authors thank Dr. Pablo Stoliar for his critical reading of this paper.

References

1. P. Martin, R. Netterfield, T. Kinder, A. Bendavid, Appl. Opt. **31**, 6734 (1992)
2. A.N. Cleland, M. Pophristic, I. Ferguson, Appl. Phys. Lett. **79**, 2070 (2001)
3. R. Bensalem, A. Abid, B.J. Sealy, Thin Solid Films **143**, 141 (1986)
4. C.C. Tin, Y. Song, T. Isaacs-Smith, V. Madangarli, T.S. Sudarshan, J. Electron. Mater. **26**, 212 (1997)
5. J. Szmidt, Chaos Solitons Fractals **10**, 2099 (1999)
6. J. Meinschien, G. Behme, F. Falk, H. Stafast, Appl. Phys. A: Mater. Sci. Process. **69**, S683 (1999)
7. Y.-J. Yong, J.-Y. Lee, J. Vac. Sci. Technol. A **15**, 390 (1997)
8. K. Kaya, H. Takahashi, Y. Shibata, Y. Kanno, T. Hirai, Jpn J. Appl. Phys. **36**, 2837 (1997)
9. T. Shiosaki, T. Yamamoto, T. Oda, A. Kawabata, Appl. Phys. Lett. **36**, 643 (1980)
10. C. Boulmer-Leborgne, A.L. Thomann, P. Andreazza, C. Andreazza-Vignolle, J. Hermann, V. Craciun, P. Echegut, D. Craciun, Appl. Surf. Sci. **125**, 137 (1998)
11. A. Guillaumot, F. Lapostolle, C. Dublanche-Tixier, J.C. Oliveira, A. Billard, C. Langlade, Vacuum **85**, 120 (2010)
12. P.-Y. Jouan, L. Le Brizoual, M. Ganciu, C. Cardinaud, S. Tricot, M.-A. Djouadi, IEEE Trans. Plasma Sci. **38**, 3089 (2010)
13. J. Musil, P. Baroch, J. Vlček, K.H. Nam, J.G. Han, Thin Solid Films **475**, 208 (2005)
14. I. Safi, Surf. Coat. Technol. **127**, 203 (2000)
15. V.S. Smentkowski, Prog. Surf. Sci. **64**, 1 (2000)
16. M. He, N. Cheng, P. Zhou, H. Okabe, J.B. Halpern, J. Vac. Sci. Technol. A **16**, 2372 (1998)
17. R.E. Sah, L. Kirste, M. Baeumler, P. Hiesinger, V. Cimalla, J. Vac. Sci. Technol. A **28**, 394 (2010)
18. O.J. Gregory, A.B. Slot, P.S. Amons, E.E. Crisman, Surf. Coat. Technol. **88**, 79 (1996)
19. W.J. Meng, J.A. Sell, G.L. Eesley, T.A. Perry, J. Appl. Phys. **74**, 2411 (1993)
20. G.G. Stoney, Proc. R. Soc. London, Ser. A **82**, 172 (1909)
21. S.R. Pulugurtha, D.G. Bhat, M.H. Gordon, J. Shultz, M. Staia, S.V. Joshi, S. Govindarajan, Surf. Coat. Technol. **202**, 1160 (2007)
22. C. Nouveau, M.-A. Djouadi, O. Banakh, R. Sanjinés, F. Lévy, Thin Solid Films **398**, 490 (2001)
23. M. Zeitler, S. Sienz, B. Rauschenbach, J. Vac. Sci. Technol. A **17**, 597 (1999)
24. Y. Watanabe, N. Kitazawa, Y. Nakamura, C. Lee, T. Sekino, K. Niihara, J. Vac. Sci. Technol. A **18**, 1567 (2000)
25. M. Placidi, J.C. Moreno, P. Godignon, N. Mestres, E. Frayssinet, F. Semond, C. Serre, Sens. Actuators A **150**, 64 (2009)
26. K. Kusaka, D. Taniguchi, T. Hanabusa, K. Tominaga, Vacuum **59**, 806 (2000)
27. S.-H. Lee, K.-H. Yoon, D.-S. Cheong, J.-K. Lee, Thin Solid Films **453**, 193 (2003)
28. F. Martin, P. Muralt, M.-A. Dubois, A. Pezous, J. Vac. Sci. Technol. A **22**, 361 (2004)
29. L. Vergara, M. Clement, E. Iborra, A. Sanz-Hervás, J.G. López, Y. Morilla, J. Sangrador, M.A. Respaldiza, Diamond Rel. Mater. **13**, 839 (2004)
30. M. Ishihara, S.J. Li, H. Yumoto, K. Akashi, Y. Ide, Thin Solid Films **316**, 152 (1998)
31. A. Sanz-Hervás, E. Iborra, M. Clement, J. Sangrador, M. Aguilar, Diamond Rel. Mater. **12**, 1186 (2003)